

## On-line Corrosion Monitoring of 70 Cu 30 Ni Alloy in a LiBr Solution under Absorption Heat Pump Flow Conditions

R. Urzúa, J. Siqueiros, L. Morales, I. Rosales, J. Uruchurtu\*

*Centro de Investigaciones en Ingeniería y Ciencias Aplicadas  
Universidad Autónoma del Estado de Morelos, México*

Received 26 September 2008; accepted 10 March 2009

---

### Abstract

Electrochemical techniques for on-line monitoring were used to study 70Cu-30Ni alloy corrosion in lithium bromide solution under flow operating conditions in an absorption heat pump. The cause of metallic corrosion on the studied alloy is the localized attack of the passive film surface by bromide ions at lower temperatures, and dissolution of the protective film at higher temperatures and flow conditions. Laboratory experiments were performed using the rotating disk electrode (RDE) under dynamic conditions and different temperatures, similar to the operating pump parameters. This was done to understand the corrosion behavior of the copper alloy prior to on-line monitoring assessment. A corrosion probe consisting in three *identical* copper alloy ring electrodes embedded in Teflon tube sections to isolate them, with the same diameter as the piping to prevent breaking down pipe flow continuity, was designed and installed. Results under various operating conditions were evaluated. Measurements obtained showed the dynamics of this industrial system and the benefits of real time monitoring in understanding corrosion behavior of 70Cu-30Ni alloy in lithium bromide solution used as working fluid and heat absorbent in heat pumps.

**Keywords:** corrosion monitoring, heat pumps, copper nickel alloy, lithium bromide.

---

### Introduction

Absorption heat pump/transformers are the only heat exchanger- recovery systems capable of increasing the waste heat temperature to make it useful in an environmental friendly way. Its main use is in operations where latent heat is discharged, especially in drying, evaporation and distillation unitary processes and in heat recovery of cooling plants.

---

\* Corresponding author. E-mail address: juch25@uaem.mx

Fig. 1 presents a schematic diagram of this system consisting basically of a generator, condenser, evaporator, absorber and a heat exchanger, as well as the electrochemical corrosion probe, as part of the heat pump piping. They use a mixture solution of two chemical substances called working fluid and absorbent, the latter with the function of transporting the working fluid from the absorption zone to the generation zone, where vapor is separated from the absorbent, for further processing and heat recovery.

The common mixture used is a 50 % w/w LiBr (absorbent)/ water(working fluid) solution, which under the system operating temperature conditions has been reported as highly corrosive for stainless steel materials, making it necessary to use corrosion inhibitors [1,2,3].

The aim of the present work is to monitor and evaluate the corrosion resistance of 70Cu-30Ni in LiBr water solution using different electrochemical techniques, for its application in absorption heat pump/transformers. On-line monitoring was also performed in order to evaluate corrosion of copper alloy under heat pump operating conditions and correlated with relevant parameters obtained under laboratory conditions.

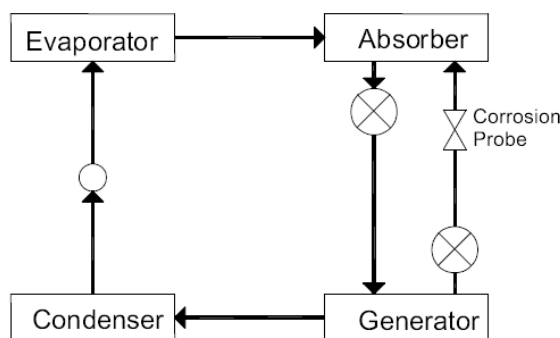


**Figure 1.** Schematic diagram for the heat pump.

### Experimental procedure

Two types of experiments were performed using electrochemical methods. Laboratory experiments under controlled conditions and corrosion monitoring in a heat pump under operating conditions.

### Solution

The corrosive solution was prepared with lithium bromide analytical grade reagents and distilled water (50 % w/w). Before preparing the aqueous solution, the solid LiBr was dehydrated in an electrical stove. 100 mL of non stirred corrosive solution were introduced into an open flask, which was placed on a mantle over a temperature/stirrer electrical stove, where the test temperature above the ambient temperature was reached. The solution was de-aerated one hour prior and throughout the experiment, bubbling nitrogen into the cell.

### Electrodes

Copper nickel alloy was obtained from pure copper and nickel melted in a ceramic crucible inside an induction furnace, with an inert argon atmosphere.

Afterwards the melting operation was repeated to obtain a homogeneous alloy and poured into a pencil like mould to obtain the specimens. Following these latter procedures, a thermal treatment was applied to the alloy. The samples were machined and 11 mm diameter cylinder bars were obtained. Also, 19 mm diameter bars obtained from the foundry were machined to manufacture the rings with 16 and 12.4 mm external and internal diameters, respectively, used for the monitoring probe.

The working electrode for the rotating disk electrode (RDE) was obtained by cylinder bars (11 mm diameter) and embedded in Teflon (PTFE); the exposure surface to the LiBr was 0.95 cm<sup>2</sup> area. A saturated calomel electrode and a graphite electrode were used as reference and auxiliary, respectively. For electrochemical current noise measurements, the tip of a platinum wire was used as counter electrode.

For on line monitoring, a three identical electrode corrosion probe was constructed from the copper alloy bar manufactured. The on-line monitoring included measurements for different temperatures obtained by means of thermo couples.

For the heat pump probe the three *identical* electrode rings were 3 mm length and 1.18 cm<sup>2</sup> exposed surface area, each one. A copper wire was soldered to each ring and they were separated by a Teflon ring to avoid electrical contact between the rings. The arrangement was embedded in a calcium epoxy resin mixture to avoid heating effects. All electrodes metal surfaces were grounded to 1500 grit silicon carbide paper, rinsed with distilled water, degreased with acetone and dried under a warm air stream [4].

The corrosion probe was installed in the absorption section exit for ease of installation or removal for substitution and/or inspection. It is possible to accommodate corrosion probes in other sections of the heat pump. The fluid solution was of industrial grade, therefore the presence of impurities such as sand can be expected and erosion corrosion is a possibility.

### ***Instrumentation and measurements***

For the sake of interpretation and to establish the copper alloy electrochemical characteristics during on-line corrosion monitoring, laboratory tests under controlled conditions were performed. Different electrochemical techniques, namely polarization curves (PC), electrochemical impedance measurements (EIS) and electrochemical noise measurements (ENM) were performed under laboratory and plant conditions. Measurements were recorded using ACM Gill 8AC software and instrumentation controlled by a personal computer. PC tests were performed from -700 mV to 100 mV at a sweep rate of 100 mV/minute. The electrochemical arrangements for laboratory conditions include the copper alloy working electrode, a saturated calomel reference electrode and a graphite counter electrode. Ohmic drop (IR) compensation for solution resistance was made by the instruments during polarization measurements. The electrochemical cell was set on a temperature/stirrer stove to perform measurements at different temperatures (25 to 60 °C) and rpm (0, 2800) rotating disk electrode conditions, equivalent to the Reynolds number in the heat pump flow. In this work, for the

three temperatures considered (25, 40 and 60 °C), the Reynolds numbers are: 4468, 6018 and 8210, respectively. LiBr density and viscosity change with temperature, therefore for 2800 rpm three different Reynolds numbers were used. EIS measurements were obtained using a 20 mV amplitude sinusoidal waveform in the frequency range from 10 kHz to 0.05 Hz. The frequency range was logarithmically swept at about 7 frequency values per decade. The integration time was measured for 10 cycles at each frequency [5, 6]. EN measurements were obtained using a three electrodes set-up. Electrochemical noise data were recorded at 1 reading/second to produce consecutive records of 1024 at different temperatures and RDE speeds. On each experiment, simultaneous measurements of potential and current noise were made. Data processing included trend removal of the signal by minimum square linear fitting.. Dividing the potential noise over the current noise, a low frequency electrochemical noise resistance was obtained, as described elsewhere [7]. Also, the localization index (LI) was obtained as the ratio between the standard deviation current and the rms current.

## Results

### *Laboratory conditions*

Fig. 2 presents potentiodynamic polarization curves for the RDE under static (blank) and flow conditions (2800 rpm), under different temperatures. The cathodic branch presents a similar behavior for all cases, with an insignificant variation in the limit current between 0.11 and 0.24 mA/cm<sup>2</sup> for all temperatures, probably associated with the limited amount of OH ions mass transport-diffusion conditions responsible for the cathodic reaction. The anodic region presents in all cases (except for 60 °C), a decrease in the current density, and a very small passive region was observed between -400 and -300 mV SCE. The passive potentials are between -380 and -340 mV SCE. This suggests that the alloy dissolution is affected by mass transport phenomena evidenced by the current limit present in the polarization curves. At room temperature (25 °C) the corrosion potential under static (blank) conditions is -410 mV SCE, showing the anodic region a small passive one at -390 mV SCE related to the corrosion products formed with a passive current of 0.7 mA/cm<sup>2</sup>, being the critical potential at about -300 mV SCE. The limit current obtained was 0.112 mA/cm<sup>2</sup>.

At room temperature but under flow conditions, the corrosion potential decreased to -478 mV SCE and a passive region started at -320 mV SCE. The limit current observed was 0.11 mA/cm<sup>2</sup>. The passive current rose to 0.0801 mA/cm<sup>2</sup>, while the critic potential obtained was at about -350 mV SCE. The limit current obtained was 0.219 mA/cm<sup>2</sup>.

At 40 °C under flow conditions, the corrosion potential is -444 mV SCE, with the anodic branch showing a passive region with a passive potential of -320 mV SCE and a passive current starting at 0.013 mA/cm<sup>2</sup>, up to the critic potential (-360 mV SCE). The limit current obtained was 0.23mA/cm<sup>2</sup>.

At 60 °C, the corrosion potential rose to about -495 mV SCE, with a current limit of 0.0291 mA/cm<sup>2</sup> and the anodic region showing free dissolution depolarizing conditions. Under this temperature and flow conditions no passive

region nor critical potential were obtained suggesting generalized corrosion, maybe due to increased solubility of the corrosion products formed, or erosion effects over the porous film over the metal surface. The limit current obtained was 0.024 mA/cm<sup>2</sup>.

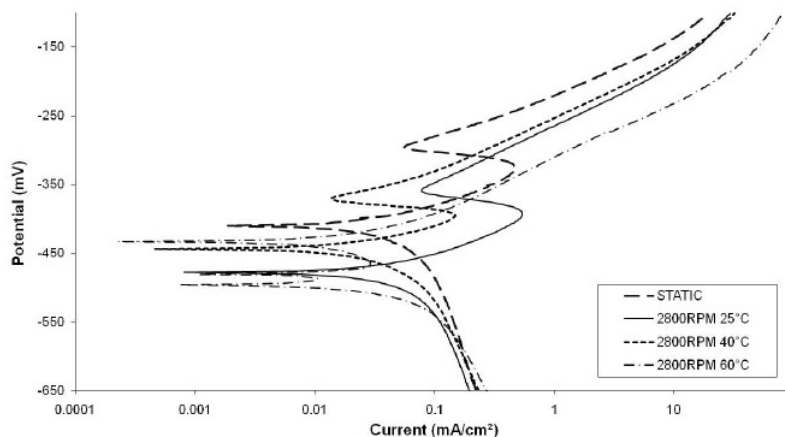


**Figure 2.** Polarization curves for static and 2800 rpm RDE at different temperature conditions.

These changes in the anodic direction appear to be related to the formation of passive corrosion products over the metal surface interfering with the metal dissolution, except at 60 °C under flow conditions. The cathodic branch presents similar slopes showing a limiting current region, which changes slightly with increasing temperature, probably associated to OH ions diffusion from slight water dissociation, showing the effect of mass transport or concentration polarization. Also, nickel electro-deposition could be expected from nickel galvanic dissolution. As the temperature is increased, there is less probability of oxygen presence due to the fact that its presence diminishes with temperature, but also the solution conductivity will change. The corrosion potential and the current limit present a trend to change as a function of temperature under RDE flow experimental conditions. The corrosion rate changes with temperature increasing as well as with flow velocity [5]. Table 1 presents the electrochemical current parameters obtained from the polarization curves under flow conditions.

**Table 1.** Electrochemical polarization current parameters at 2800 rpm.

Temperature °C	$i_{\text{corr}}$ mA/cm <sup>2</sup>	$i_{\text{pass}}$ mA/cm <sup>2</sup>	$i_{\text{limit}}$ mA/cm <sup>2</sup>	$i_{\text{critic}}$ mA/cm <sup>2</sup>
25 (static)	0.050	0.071	0.11	0.075
25	0.081	0.080	0.21	0.090
40	0.040	0.013	0.23	0.015
60	0.048	-	0.24	-

Fig. 3 presents an analogous Arrhenius plot for the limit current density in a logarithmic scale as a function of the inverse temperature (1/T), where a linear relation can be observed with a regression coefficient of 0.99 for the three temperatures studied at 2800 rpm.

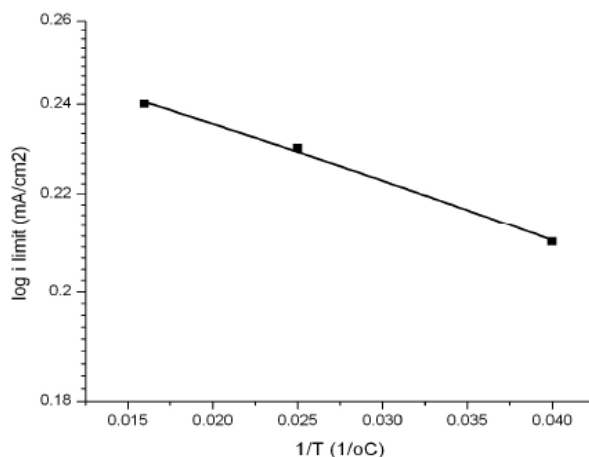


**Figure 3.** Limit current density as a function of  $1/T$  at 2800 rpm.

### **Impedance**

Experimental and simulated Nyquist impedance plots, using equivalent circuit, of copper alloy in bromide solution under static (blank) and rotating conditions for different temperatures, are shown in Fig. 4. All Nyquist impedance plots obtained at corrosion potential are similar, composed of three depressed semicircle segments with similar time constants (RC). These can be modeled in terms of parallel resistances and constant phase elements associated to surface roughness. This is a circuit usually used for metals with a passive or porous film [9]. Electrochemical parameters have been calculated from the obtained impedance data simulation using Z view software [9], and presented in Table 2. R1 is associated to the pore defects of the film present on the surface, R2 is the film resistance and R3 the charge transfer resistance. The CPE are the constant phase elements associated, and  $n$  is a parameter taking values between 0 and 1 depending on the circuit element represented. Values close to 1 represent an ideal capacitance, and the parameter is associated to the heterogeneities of the metal surface.

**Table 2.** Equivalent circuit fitting parameters.

Parameters	0 RPM		2800 RPM	
	25	25	40	60
Rs (ohms)	1.619	1.548	1.375	1.127
CPE1(Farads)	5.046E-5	5.4932E-5	6.7575E-5	8.6195 E-4
n1	0.88865	0.91143	0.88398	0.69068
R1 (ohms-cm <sup>2</sup> )	262.6	231.4	87.83	23
CPE2(Farads)	4E-5	0.00027792	0.00041754	3.5275 E-6
n2	0.8952	0.62117	0.64775	0.42
R2 (ohms-cm <sup>2</sup> )	313.8	849.7	329.8	53.01
CPE3(Farads)	0.0002831	0.0001678	0.009905	1.5226 E-3
n3	0.68193	0.696	0.43436	0.54035
R3 (ohms-cm <sup>2</sup> )	1216	31.49	14.45	45

It can be seen that the total real impedance decreases as a function of temperature for dynamic, as compared to static conditions. The three semicircle arches, presented in the impedance plot are as follows: The first capacitive semicircle is associated to the pores or defect sites in the oxide film [6, 8], while the second capacitive semicircle is probably associated to the passive oxide film formation reaction [8]. The third semicircle corresponds to the charge transfer resistance. The time constants (RC) associated to the three semicircle segments appear to be similar, therefore the appearance of one depressed semicircle [6-9].

Fig. 5 presents the electrical equivalent circuit used to fit the electrochemical data obtained (Fig. 4) and the parameters are presented in Table 2.

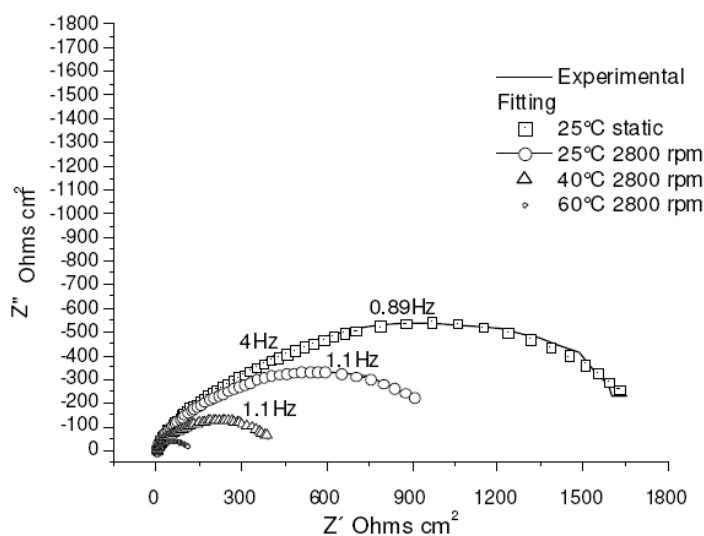


**Figure 4.** Nyquist diagrams at 2800 rpm.

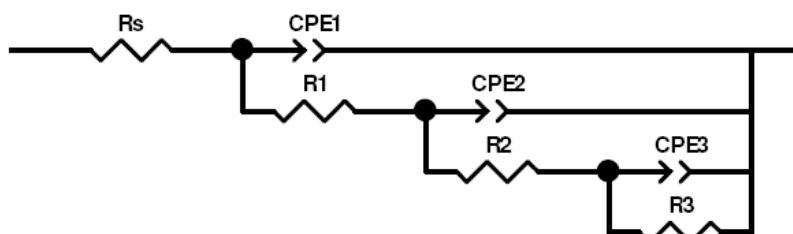


**Figure 5.** Equivalent circuit fitting.

It can be seen that  $R_1$  and  $R_2$  decrease as a function of temperature, related to the porous condition of the passive film.  $R_3$  decreases at 40 °C, increasing again at 60 °C, reflecting the changes of the corrosion rate in the presence and the absence of the passive oxide film.

### ***Electrochemical noise***

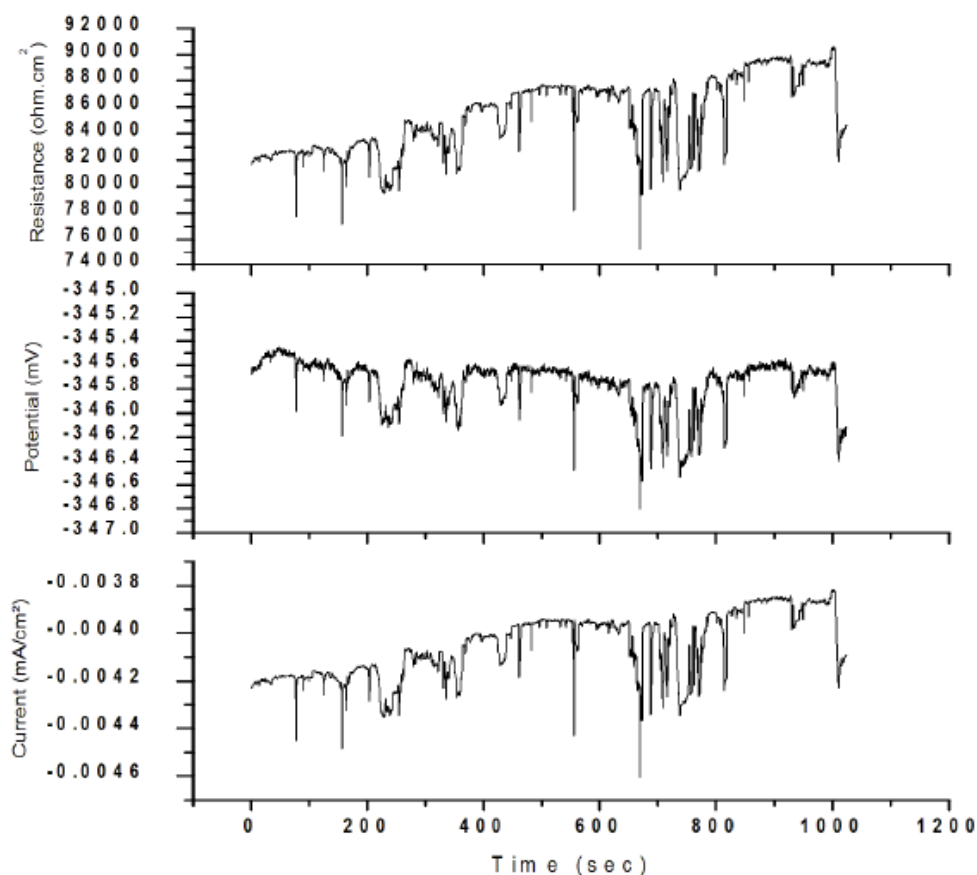
Fig. 6, 7 and 8 present the electrochemical potential and current noise and the resistance obtained as the ratio of the two, for the different dynamic and temperature conditions tested with the RDE. At 25 °C, the potential and the current noise time series showed the typical film rupture repassivation transients associated to pitting initiation and propagation events. The noise resistance for overall corrosion increased as a function of time during this experiment. It rose

from 80 to 90 Kohms-cm<sup>2</sup>. Similar behavior was observed for static conditions at room temperature, as seen in Fig. 6.

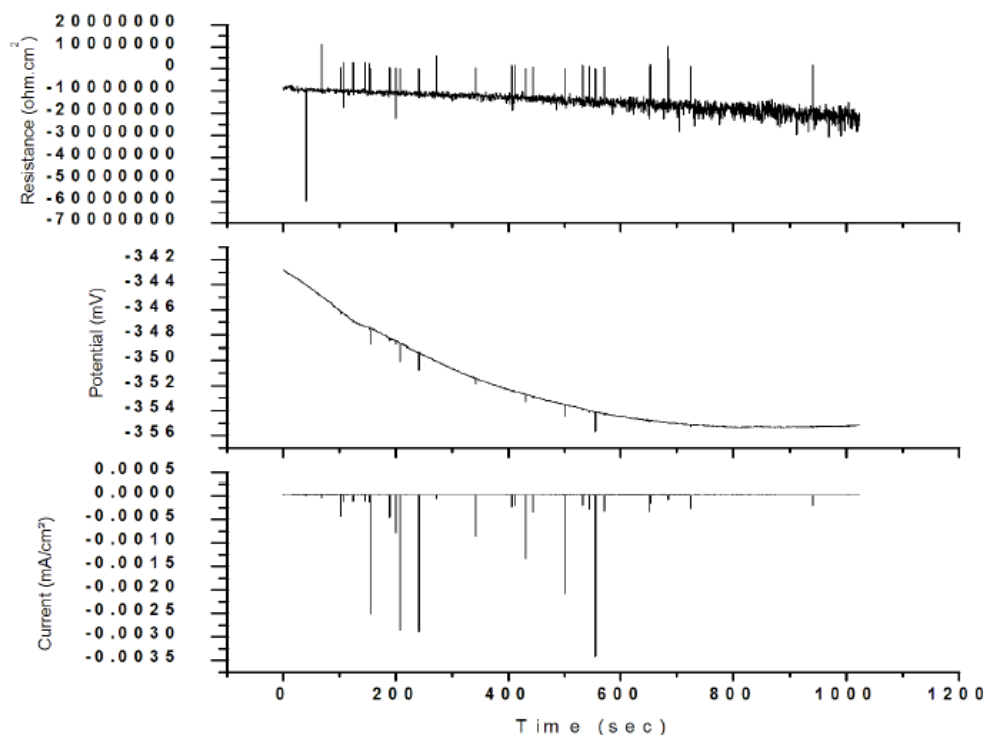
At 40 °C (Fig. 7) the potential and current noise time series showed mixed behavior: few sudden transients superimposed to low amplitude high frequency oscillations associated to mixed conditions: general and localized corrosion [7,10-12]. The noise resistance rose from 10 to 30 Mohms-cm<sup>2</sup>.

Fig. 8 presents the potential and current noise time series and noise resistance at 60 °C, under dynamic conditions. The noise time series present high amplitude low frequency with superimposed low amplitude high frequency oscillations, associated to generalized corrosion under diffusion control [13]. The noise resistance oscillated between 500 Kohms-cm<sup>2</sup> and 3 Mohms-cm<sup>2</sup>.

Differences observed at the different temperatures are clear. The results suggest changes from localized to mixed to generalized corrosion as temperature is raised under dynamic rotating conditions. This was confirmed during corrosion monitoring in the heat pump (see Fig. 14). Corrosion initiation at the tested copper alloy proceeds by galvanic nickel dissolution, probably at local sites in the form of localized pitting, as evidenced by the electrochemical noise results obtained [11]. Some nickel electro-deposition and film formation occur, except for the higher temperature, where the passive film is prevented, probably due to corrosion products solubility under this condition.



**Figure 6.** Potential, current noise time series and noise resistance at 25 °C and 2800 rpm.



**Figure 7.** Potential, current noise time series and noise resistance at 40 °C and 2800 rpm.

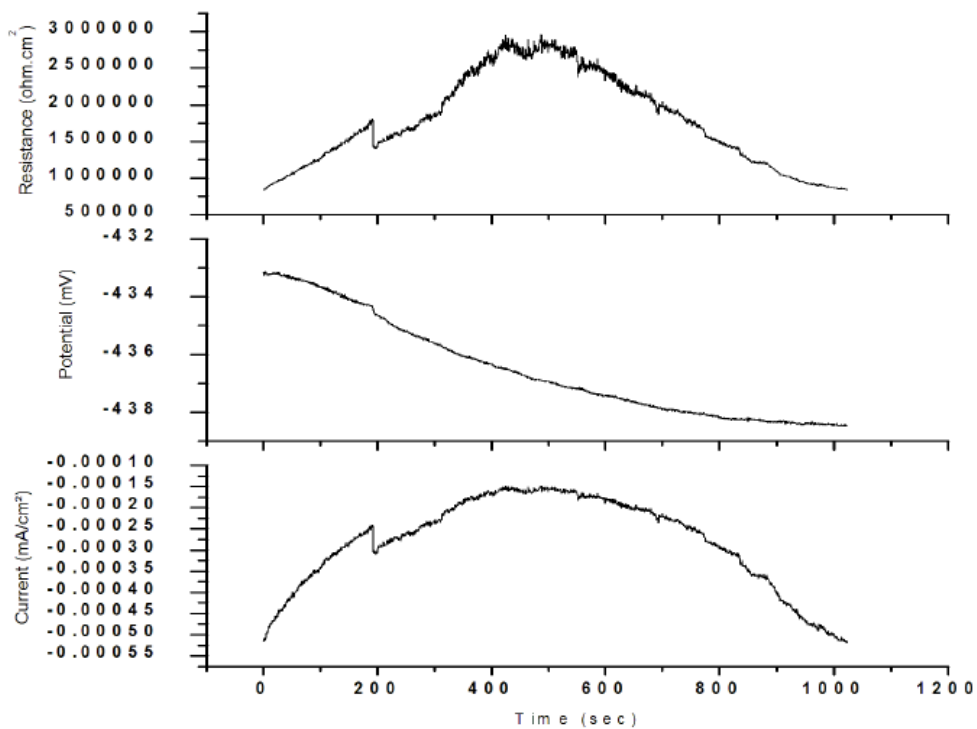


**Figure 8.** Potential, current noise time series and noise resistance at 60 °C and 2800 rpm.

### ***On-line corrosion monitoring***

Fig. 9 reports the installed corrosion probe and a schematic diagram, representing the absorption heat pump used to monitor the copper alloy corrosion under real operating conditions. The circuit design focused (see Fig. 1) on the electrochemical cell, consisting in three *identical* copper alloy ring electrodes embedded in Teflon tube sections to isolate them, the same diameter as the piping to prevent breaking down pipe flow continuity (Fig. 9). The three rings were used for electrochemical measurements acting as working, counter and auxiliary electrodes, applying the Sereda modified technique [14].

The probe was installed at the heat pump generator outlet, with a working flow of 4.5 liters/sec. Sequential LPR impedance, impedance and electrochemical noise measurements were performed, from the start-up till pump shut-down. Also polarization curves were obtained at the start and at the end of the run. The starting temperature was 25 °C, and 70 °C at shutdown.

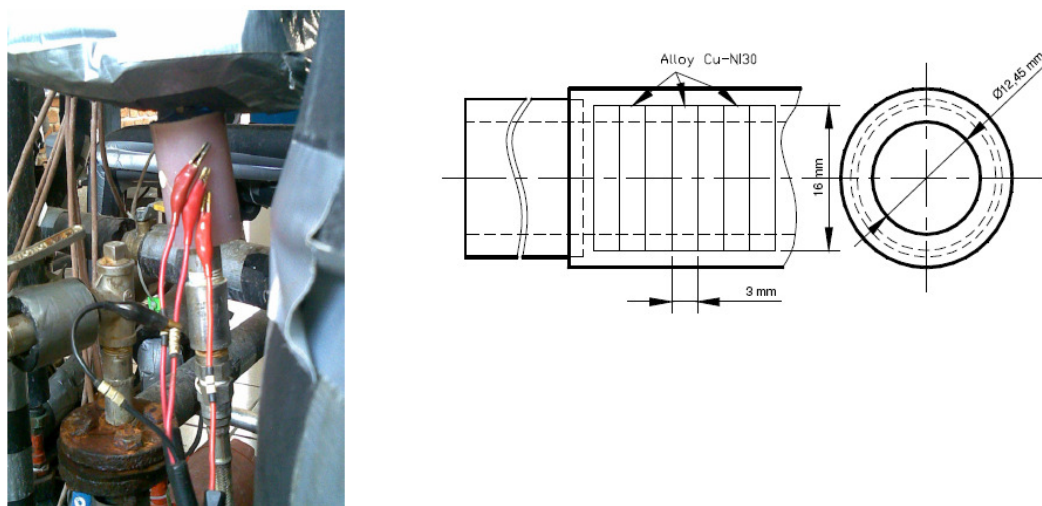


**Figure 9.** Corrosion probe and schematic diagram representing the electrochemical probe.

Fig. 10 presents the polarization curves for the absorption heat pump for start-up and shut-down conditions. They present similar corrosion potentials, while the start-up temperature presents a very small passive region as compared to the shut-down at higher temperature condition, presenting an active corrosion products polarizing region. Nevertheless the slopes in both branches appear very similar for the two conditions, suggesting similar corrosion kinetics for both cases.

### ***Impedance***

As an example, **Fig. 11** presents experimental and simulated Nyquist plots obtained during on-line corrosion monitoring, using the same circuit as before. The graphs are similar to the ones obtained under laboratory conditions. They consisted of three depressed capacitive semicircles, associated to the charge transfer, film formation and porous film condition, as explained above. At higher temperatures during shut down, the third semicircle is not complete, probably due to diffusion adsorption effects.

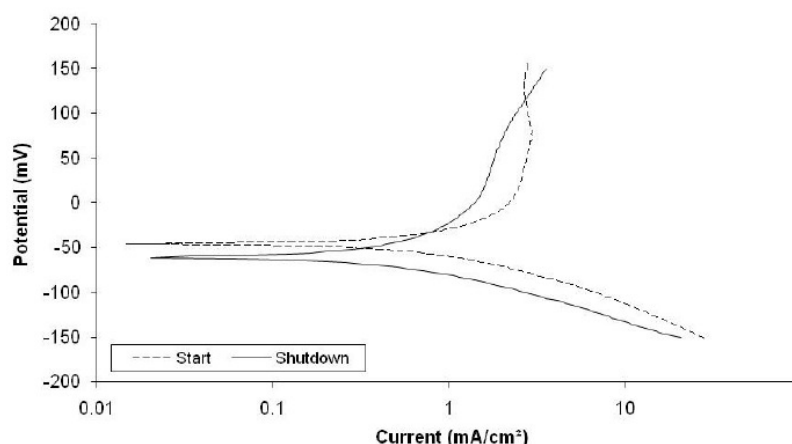


**Figure 10.** On-line polarization curve at start-up and shut-down conditions.

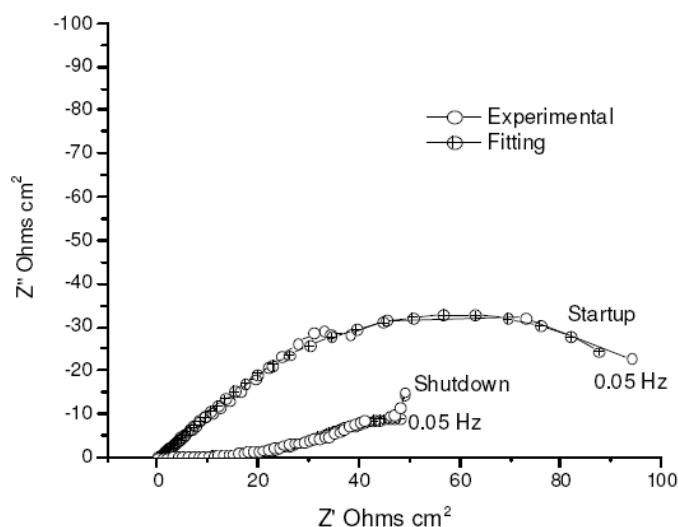


**Figure 11.** Heat pump impedance at start-up and shut-down.

The simulation values for the equivalent circuit are presented in Table 3. The impedance values suggest an increase in the corrosion rate under higher temperature operating and shut down conditions, as well as under laboratory conditions.

### ***Electrochemical noise***

As an example, Fig. 12 and 13 present electrochemical potential, current and noise resistance as a function of time, obtained during heat pump start-up and shut-down operating conditions. Transient behavior was observed with an average noise resistance of 400 Kohms-cm<sup>2</sup>, and 250 Kohms-cm<sup>2</sup> for the shut down condition. This suggests the presence of a protective film over the surface, before temperature increasing and localized corrosion as the main form of attack, for the start up condition.

**Table 3.** On-line experimental and simulated impedance values.

Parameters	Heat Pump	
	Start-up	Shut-down
$R_s$ (ohms $\text{cm}^2$ )	0.51415	0.4740
CPE1 (Farads)	0.0023799	0.001156
n1	0.60405	0.8625
$R_1$ (ohms- $\text{cm}^2$ )	44.31	2.023
CPE2 (Farads)	0.00043792	0.024988
n2	0.85902	0.46942
$R_2$ (ohms- $\text{cm}^2$ )	373.17	50.75
CPE3 (Farads)	0.0041958	0.00064562
n3	0.6932	0.67
$R_3$ (ohms- $\text{cm}^2$ )	41.44	9.474

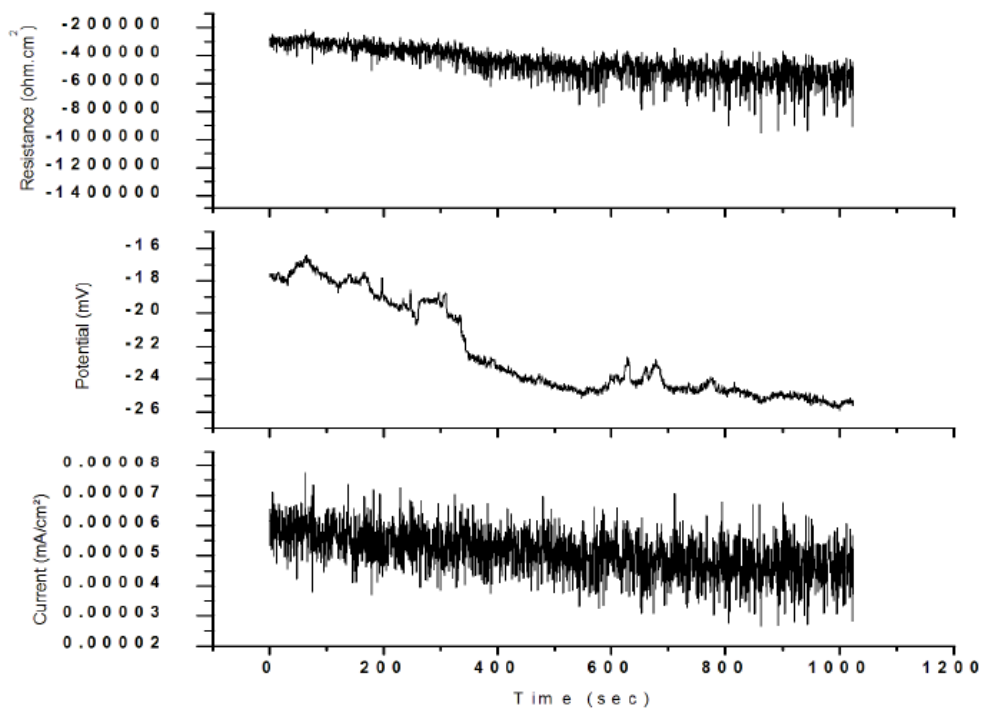
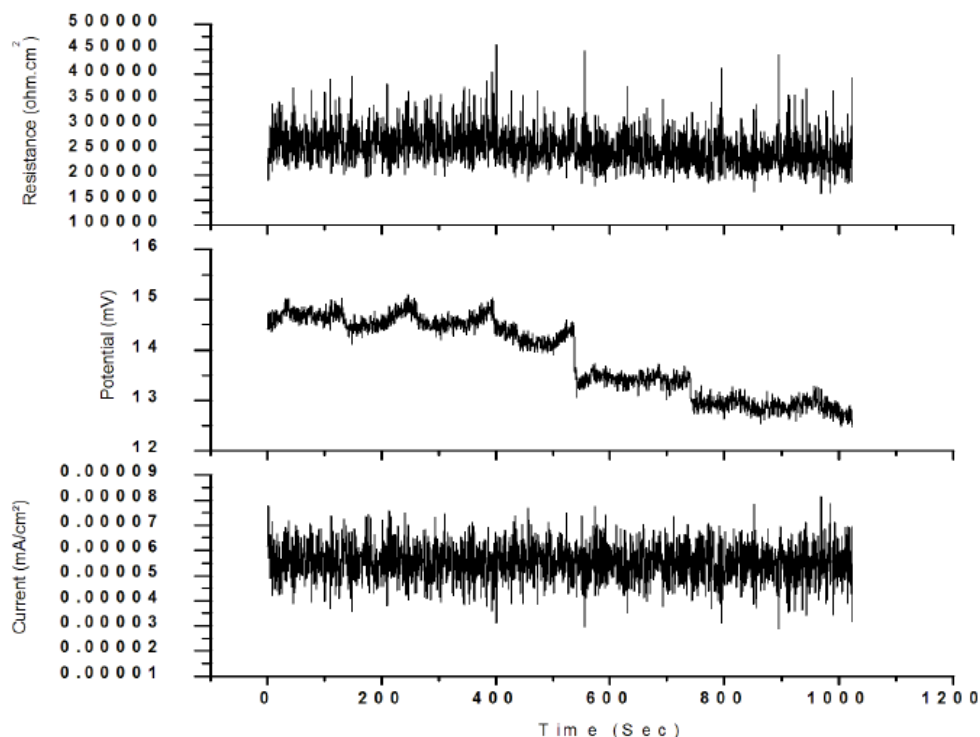
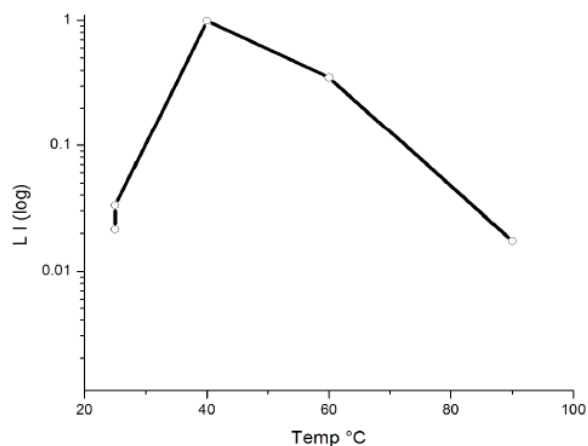
**Figure 12.** Electrochemical noise time series during start-up.

Fig. 14 presents the electrochemical noise localization index (LI) as a function of operating temperature, obtained during on-line corrosion monitoring. The value lies between 0.001 and 0.01 for passive or generalized, 0.01 and 0.1 for mixed and 0.1 and 1 for localized attack. Two values for ambient temperature are presented, corresponding to static and dynamic conditions. Obtained values suggest that localized attack is taking place between 40 and 60 °C, while mixed attack is present below and above these temperatures [11, 14].



**Figure 13.** Electrochemical noise time series during shut-down.



**Figure 14.** On-line electrochemical noise localization index.

On-line corrosion monitoring as a function of time and temperature is presented in Fig. 15. Also, the heat pump inlet and outlet temperatures were monitored, with thermo-couples installed in the heat pump. Noise resistance and LPR linear polarization resistance values are presented, and compared with the different temperatures registered for operating flow conditions. The current density as a function of time obtained from LPR, is presented in Fig.14.

The inlet and outlet temperatures increase during start-up, reaching a steady state operating condition at about 90 °C, and decreasing during shut down conditions, obtaining waste heat, for further processing and heat recovery. The noise resistance as a function of time presents oscillations in its value, probably due to film formation and rupture during start-up. It rose from 0.9 Kohms-cm<sup>2</sup> up to 1 Mohms-cm<sup>2</sup> and reaching steady state conditions around 100 Kohms-cm<sup>2</sup>.

During shut-down the noise resistance rose again to around 1 Mohms-cm<sup>2</sup>. The  $i_{\text{corr}}$  obtained from the LPR measurements oscillated between 10 mA/cm<sup>2</sup> and 0.002 mA/cm<sup>2</sup>, reaching steady state operating conditions, around 0.05 mA/cm<sup>2</sup>. At shut-down the corrosion current density diminished to 0.002 mA/cm<sup>2</sup>. Both electrochemical parameters showed a direct relation with the operating heat pump temperature conditions.

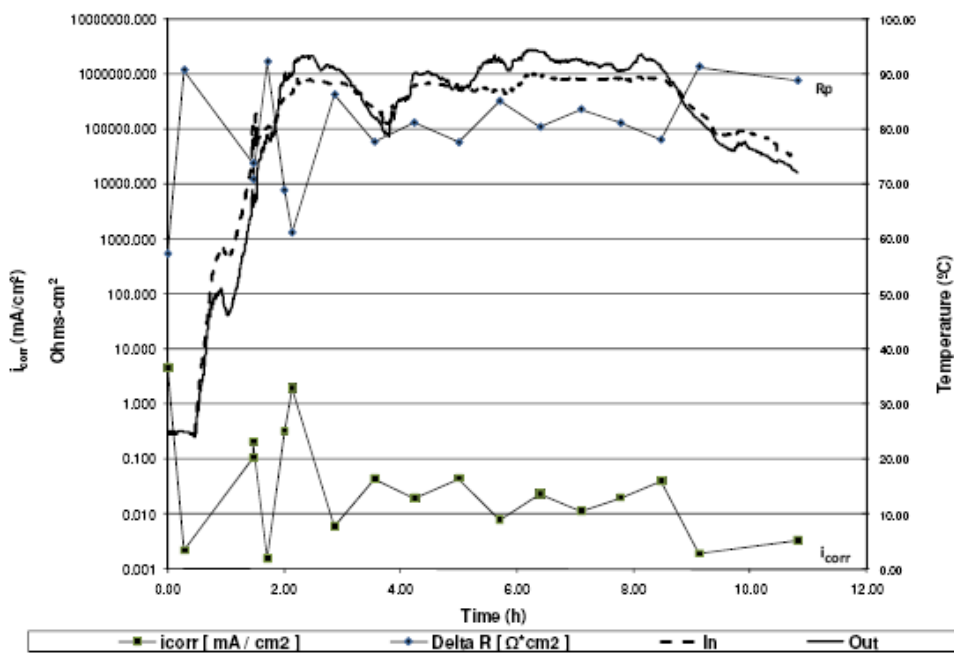


**Figure 15.** On-line corrosion monitoring parameters as a function of time.

From the electrochemical results obtained, the dissolution of the copper alloy under flow conditions is governed by mass transport of nickel ions from the electrode surface to the bulk solution through the protective film and the diffusion layer. Also, a certain effect of fluid velocity on corrosion would be expected as a result of changes in hydrodynamics, and a general dependence of corrosion rate on fluid velocity, as suggested [15]. A general dependence was established [15] between the corrosion limit current density and Reynolds number, as follows:

$$i_{\text{lim}} = K * \text{Re}^n$$

The experimental exponent in the equation lies in the range between 1 and 3 depending upon the corrosion mechanism and flow regime. For simple mass transport in the inside wall of the tube the value is close to 1, while for erosion corrosion in particle containing liquids (industrial conditions) is near to 3. For mixed control of a chemical step and mass transport, its value varies between 0 and 1 depending on the mass transport. For values between 1 and 3, there is a mixed control of mass transport and erosion corrosion [15, 16, 17].

For pure copper corrosion in LiBr solution a constant value of 1.48E-4 and an exponent value of 1.06 is reported [15]. In our case, for 25 °C and 4467 Reynolds number, the exponent value obtained was 0.01, suggesting a mass transport

corrosion control. However, some difficulties could arise in determining the corrosion mechanism simply from the values of the exponent. Nevertheless, electrochemical results obtained suggest a mass transport control as well.

### Conclusions

Results obtained demonstrate the applicability of electrochemical monitoring techniques in the study and monitoring of corrosion phenomena. Corrosion activity weakly depends on flow and temperature conditions. Corrosion of 70 copper 30 nickel alloy starts as galvanic dissolution of nickel and passive film formation over the metal surface.

Localized corrosion promoted by bromide ions appears to be the main form of attack for lower temperatures up to 40 °C in the presence of a passive film, while mixed or general corrosion is the main form of attack at higher temperatures, probably due to high solubility of corrosion products at these temperatures. The corrosion mechanism of 70Cu-30Ni alloy in lithium bromide solution is controlled by passive film and mass transport, according to the electrochemical results obtained.

For heat pump corrosion monitoring, electrochemical noise localization index suggests that corrosion attack is mixed and localized and erosion corrosion conditions do exist due to impurities present in the fluid solution.

Electrochemical methods complemented corrosion information and helped to establish the most aggressive conditions encountered during plant operation. Results underlined the dynamics of the corrosion phenomena and the usefulness of on-line corrosion monitoring.

### Acknowledgements

Authors thank Dr. David Ponce from Metallurgy Laboratory and M.Sc. Carlos Moo Chale, M.Sc. A. Huicochea and Ing. A. Horacio Hernandez S. Thermal Laboratory of UAEM-CIICAp.

### References

1. J.W. Furlong, *Air Pollut. Consultant* 11/12 (1994) 112.
2. U. Lotz, E. Heltz, *Werkst. Korros.* 34 (1983) 454.
3. P. Druska, H.H. Strhblow, S. Golledge, *Corros. Sci.* 38 (1996) 835.
4. ASTM G 3-89(2004) "Standard Practice for Conventions Applicable to Electrochemical Measurements in Corrosion Testing", Annual Book of ASTM Standards.
5. V. Pérez-Herranz, M.T. Montanes, J. García, J.L. Guiñon, *Corrosion* 57-10 (2001) 835.
6. S.R. Taylor, E. Gileadi, "Physical interpretation of the Warburg impedance", *Corrosion* 51 (1995) 664-671.
7. E. Garcia, J. Uruchurtu and J. Genesca, *Revista de Metalurgia, CENIM*, October (1995) 307.

8. W.H. Smyrl, *Electrochemical Corrosion Testing ASTM STP 727*, Fiorian Mansfeld and Ugo Bertocci, ASTM (1981) 198.
9. Zplot and Zview, Scribner Associates, Inc., Operation Manual.
10. J. Tan, S. Bayley, B. Kinsella, "The Monitoring of Formation and Destruction of Corrosion Inhibitor Films using Electrochemical Noise Analysis (ENA)", *Corros. Sci.* 38(10) (1996) 1681-1695.
11. J. Dawson, "Electrochemical Noise Measurements: The Definitive In-situ Technique for Corrosion Applications", ASTM STP 1277 (J. Kearns, J. Scully, P. Roberge, D. Reichert, J. Dawson, Eds. 1996) Philadelphia, 3-35.
12. R. Kelly, M. Inman, L. Hudson, "Analysis of Electrochemical Noise for Type 410 Stainless Steel in Chloride Solution" ASTM STP 1277, J. Kearns, J. Scully, P. Roberge, D. Reichert, J. Dawson, Eds. 1996) Philadelphia, 101-113.
13. J. Uruchurtu and J.M. Malo, *Trends in Corrosion Research* 2 (1997) 49.
14. P.J. Sereda, *ASTM Bulletin, ASTM, Philadelphia* 28 (1958) 53-55.
15. G.J. Bignold, K. Garbett, R. Garnsey, I.S. Woosley, *Water Chem. Nucl. React. Syst.* 2 (1981) 5.
16. E. Heltz, *Electrochim. Acta* 41-4 (1996) 503.
17. M.M. Stack, F.H. Stott, G.C.Wood, *J. Phys. IV* 3 (1993) 687.